THE JOURNAL OF PHYSICAL CHEMISTRY C

Article

Cite This: J. Phys. Chem. C 2019, 123, 7225−7229

pubs.acs.org/JPCC

Silicene-Like Domains on $IrSi_3$ Crystallites

Dylan Nicholls, Fatima, Deniz Çakır, and Nuri Oncel*

Department of Physics and Astrophysics, University of North Dakota, Grand Forks, North Dakota 58202, United States

ABSTRACT: Recently, silicene, the graphene equivalent of silicon, has attracted a lot of attention because of its compatibility with Si-based electronics. So far, silicene has been epitaxially grown on various crystalline surfaces such as Ag(110), Ag(111), Ir(111), ZrB_2(0001), and Au(110) substrates. Here, we present a new method to grow silicene via high-temperature surface reconstruction of hexagonal $IrSi_3$ nanocrystals. The h-$IrSi_3$ nanocrystals are formed by annealing thin Ir layers on the Si(111) surface. A detailed analysis of the scanning tunneling microscopy images shows the formation of silicene-like domains on the surface of some of the $IrSi_3$ crystallites. We studied both morphology and electronic properties of these domains by using both scanning tunneling microscopy/spectroscopy and first-principles calculation methods.

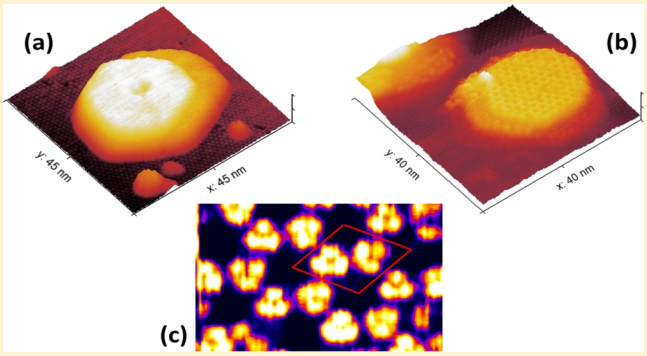

INTRODUCTION

Graphene has attracted a lot of attention for its unique properties, which include excellent electrical/thermal conductivity and strong mechanical strength.[1,2] The immediate alternatives for graphene are from the other group IV elements in the periodic table with the similar electron configuration, that is, silicon (Si) and germanium (Ge).[3] Although all three elements have four electrons in their outermost s- and p-orbitals, energetically, the most favorable crystal structure of Si and Ge is the diamond structure.[4] Therefore, for Si and Ge, graphite-like allotropes (hereafter referred as silicene and germanene) do not exist in nature. Hence, silicene and germanene have to be synthesized. The term "silicene" was introduced by Guzmán-Verri and Lew Yan Voon in 2007 to refer to the two-dimensional structure of silicon atoms in a honeycomb arrangement.[5] Takeda and Shiraishi were the first to predict the possibility of a stable single sheet of Si.[6] In that paper, the authors predicted that silicene will not be flat but puckered. Further, theoretical calculations on free-standing silicene showed that this two-dimensional system can be stable with properties similar to graphene such as linear dispersion with the Dirac cone at the corner of the Brillouin zone.[7−9] Theoretical studies also showed that the spin−orbit coupling strength is much larger in silicene than that in graphene which can make the quantum spin Hall effect detectable experimentally.[10]

Silicene's novel properties predicted by theorists and its relatively easy integration into the current semiconductor technology motivated some experimental groups to start working on growing silicene. The very first silicene was grown on Ag(110) and Ag(111) surfaces.[11−20] Recently, it has been shown that silicene can be grown on Ir(111),[21] ZrB_2(0001), and[22] Au(110)[23] substrates. One of the most studied silicene systems is silicene/Ag(111). Owing to the interaction between silicene and the substrate, the bucking pattern of Si atoms is rearranged resulting in various superstructures such as (4×4), $(\sqrt{13} \times \sqrt{13})R13.9°$, and $(2\sqrt{3} \times 2\sqrt{3})$, [with respect to the Ag(111) surface lattice] and (3×3) [with respect to silicene (1×1)].[24−26] All these superstructures show slightly different honeycomb configurations. ARPES measurements on 4×4-silicene along the Ag $\bar{\Gamma}-\bar{K}$ direction through the silicene $\bar{K}$ point show a downward dispersing branch of the honeycomb silicene bands. The dispersion is similar to the dispersion of graphene around the $\bar{K}$ point, indicating that electrons behave as massless Dirac fermions.[27] ARPES measurements on $\sqrt{3} \times \sqrt{3}$-silicene exhibit Λ- and V-shaped linear π and π^* silicene bands at the $\bar{\Gamma}_0$ point along the $\bar{\Gamma}-\bar{K}$ silicene direction.[28]

Another method to grow silicene or germanene is to use high-temperature surface reconstruction of metal silicides/germanides.[29,30] In this paper, we show that the deposition of a few monolayers of Ir on Si(111) followed by annealing at 750 °C leads to the formation of $IrSi_3$ nanocrystals. Scanning tunneling microscopy (STM) images of these crystallites show a surface reconstruction with a buckled honeycomb structure that resembles previously reported silicene-like regions on $MoSi_2$ crystallites supported on Si(001).

EXPERIMENT

The Si(111) samples used in the STM experiments were cut from nominally flat 76.2 mm by 0.38 mm, single side-polished n-type (phosphorous doped) wafers. The samples were mounted on molybdenum holders, and the contact of the

Received: January 18, 2019
Revised: February 21, 2019
Published: March 7, 2019

DOI: 10.1021/acs.jpcc.9b00550
J. Phys. Chem. C 2019, 123, 7225−7229

samples to any other metal during preparation and experiment was carefully avoided. The STM/STS studies have been performed by using an ultrahigh vacuum system with a base pressure of 2×10^{-10} mbar equipped with an Omicron Variable Temperature STM and an LK technologies RVL2000 LEED-Auger system. Before introducing Si(111) samples into the UHV chamber, samples were washed with isopropanol and dried under the flow of nitrogen gas. Si(111) samples were degassed extensively and then flash-annealed at 1250 °C. The sample temperature was measured with a pyrometer. The quality of the clean Si(111) samples was confirmed both with LEED and STM prior to Ir deposition. Ir was deposited on the clean Si(111)-7 × 7 surface kept at room temperature from a current-heated Ir wire (99.9%) with a standard deposition rate of 2.8×10^{-4} nm/s. Then, the sample was annealed at 750 °C to form $IrSi_3$ nanocrystals. All the STM experiments were performed at room temperature. $I-V$ curves measured at all points of the image while measuring high-resolution STM images of the surface. The measured $I-V$ curves were then averaged. The local density of state curves $(\mathrm{LDOS}-(\mathrm{d}I/\mathrm{d}V)/(I/V))$ were calculated out of the $I-V$ curves.

COMPUTATIONAL DETAILS

We performed first-principles calculations based on the density functional theory as implemented in the Vienna Ab initio Simulation Package (VASP).[31,32] We described the ions by employing PAW pseudopotentials for the atomic core region.[33] The generalized gradient approximation was used for the exchange−correlation functional within the Perdew−Burke−Ernzerhof formulation.[34] The kinetic energy cutoff for plane-wave expansion was set to 400 eV. We used 3 × 3 × 1 and 5 × 5 × 1 k-point meshes for relaxation and density of state calculations, respectively.[35] The [0001] surface of hexagonal $IrSi_3$ (with a space group of $P6_3/mmc$) was modeled by a slab with a thickness of 15 Å. The convergence criteria for the total energies were chosen as 10^{-5} eV between the consecutive ionic steps, and the maximum force allowed on each atom was set to 0.01 eV/Å. Bottom layer Si atoms were terminated by hydrogen atoms in order to saturate the dangling bonds and we kept their positions fixed during structural relaxations. A vacuum region of 15 Å was introduced in order to prevent spurious interactions between the periodic slabs along the z direction. Only the top three atomic layers were allowed to relax and reconstruct, and remaining layers were fixed at their corresponding bulk atomic positions in the calculations.

RESULTS & DISCUSSION

We first realized the formation of silicene-like domains while studying the morphology of the Ir-modified Si(111) surface at relatively high Ir coverages (>1 ML). We choose to call our system as silicene-like domain (SLD) and avoid calling it silicene without experimental proofs showing that SLD's are electronically decoupled from the substrate. Figure 1a,b shows large-scale STM images of the surface with these islands. The islands were on different samples but grown under the same conditions. The islands are similar in size and shape; however, island in Figure 1b have SLD's, whereas the island in Figure 1a is flat and featureless. The wetting layer surrounding the island is made out of Ir-ring clusters that form $\sqrt{7} \times \sqrt{7}$ domains on Si(111).[36,37] Ring clusters consist of a transition metal surrounded by six Si atoms, three of which directly bind to the transition metal and are called bridging adatoms and the

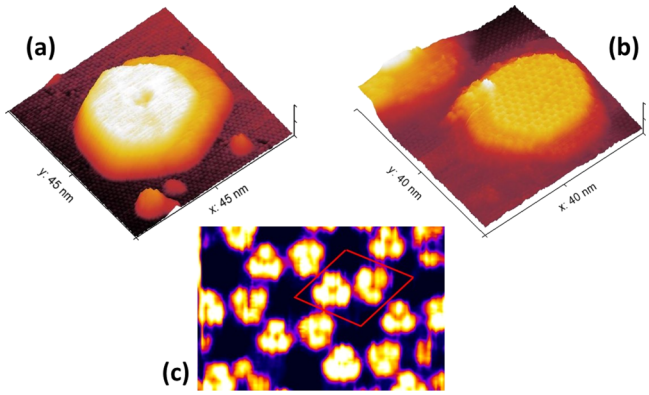

Figure 1. (a,b) are STM images of $IrSi_3$ crystallites with no SLD and SLD on top, respectively. For a(b), the sample bias and the tunneling current are −1.7 V (−1.36 V) and 0.32 nA (0.43 nA), respectively. (c) 5.3 nm × 8 nm STM image of the silicene-like domains. Red rhombus marks the unit cell. The edges of the red rhombus are parallel to the $\sqrt{7} \times \sqrt{7}$ unit cell of Ir-ring clusters. The size of the unit cell is 23.1 Å which corresponds to $2\sqrt{7} \times 2\sqrt{7}$ with respect to 1 × 1 of the Si(111) surface. For (c), the sample bias and the tunneling current are −1.5 V and 0.43 nA, respectively.

remaining three Si atoms, called the capping adatoms bind two bridging adatoms and one Si substrate atom. The Ir/Si(111) system exhibits Stranski−Krastanov-type growth. The Ir-ring clusters function as a wetting layer, and further deposition of Ir leads to the formation of the islands. The STM image in Figure 1c shows a higher-resolution picture of an SLD. The unit cell is indicated by a red rhombus enclosing a total of six protrusions, three per half unit cell. The size of the unit cell is 23.1 Å.

There are previous studies on bulk properties of iridium silicides epitaxially grown on various Si surfaces.[38−40] Ir−silicides have three known crystal phases (IrSi, Ir_3Si_5, and $IrSi_3$), which can be grown selectively, and each phase grows in a specific temperature range. Among those phases, IrSi and $IrSi_3$ are metallic and Ir_3Si_5 is a semiconductor with a band gap of about 1.2 eV.[41] The phase diagram of the bulk Ir−Si system is eutectic at 1222 °C and at a composition of 80.5% Si and 19.5% Ir.[42] The $IrSi_3$ phase is the phase closest to the bulk eutectic composition. When the eutectic droplet cools down, it goes through spinodal decomposition and two stable phases emerge, Ir-free Si (forms the bulk Si) and $IrSi_3$. Owing to relatively small Ir coverage on the surface (1−2 ML), the current system follows the phase diagram on the Si-rich side. However, the temperatures at which $IrSi_3$ forms are much lower than that of the bulk eutectic point. We attributed this to the fact that for nanostructures, both solidus and liquidus curves shift to lower temperatures than that of the bulk phase diagram.[43,44] A similar shift of the eutectic point to lower temperatures has been observed in vacuum−liquid−solid growth of Ge nanowires when the catalyst was super-saturated.[45] Lin et al. grew $IrSi_3$ on Si(111) at much lower temperature (ranging from 630 to 800 °C) than the eutectic point by co-depositing Ir and Si on Si(111) in the stoichiometric ratio.[46] They reported the growth of three major modes (A, B, and C) of epitaxial silicides. Each mode of growth refers to a specific set of the orientation relation between $IrSi_3$ and the Si(111) substrate.[47] Silicides grown at 630 °C exhibited two types (A and B) with approximately 50% of the area covered by each mode and 100% of the surface covered with Si. On the other hand, for $IrSi_3$ layers grown at

DOI: 10.1021/acs.jpcc.9b00550
J. Phys. Chem. C 2019, 123, 7225−7229

780 °C, epitaxial island formation of type C which covers approximately 70% of the surface was observed. Among these modes of growth, mode A and mode C are vicinal surfaces and cannot explain the formation of SLDs. However, mode B corresponds to the growth of [0001] of $IrSi_3$ parallel to [111] of Si. On the basis of Lin et al.'s paper and the STM images we measured, we chose to use the [0001]-terminated surface of $IrSi_3$ for DFT calculations (Figure 2). $IrSi_3$ has a hexagonal

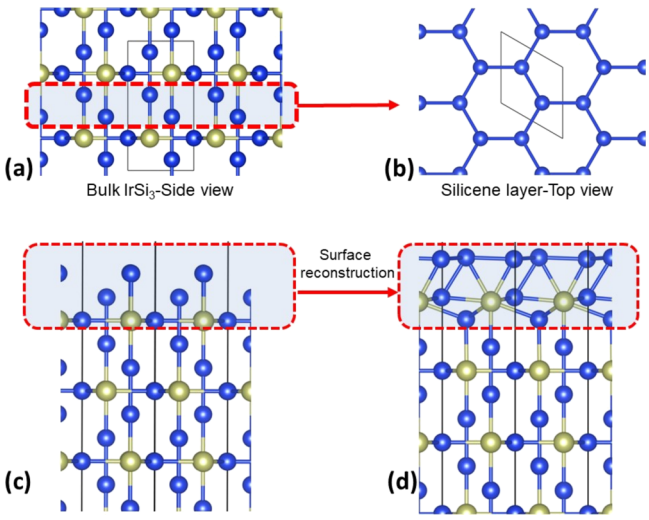

Figure 2. (a) Side view of bulk $IrSi_3$. Si and Ir atoms are represented by blue and yellow balls, respectively. We mark two silicon layers, which were used to terminate the $IrSi_3$ (0001) surface in our calculations. (b) Top view of these silicon layers resembles silicene. (c) Unrelaxed and (d) relaxed structure of the $IrSi_3$(0001) surface. Surface reconstruction gives rise to a significant reorganization of the silicon atoms at the surface.

crystal structure with a = 4.37 Å and c = 7.40 Å.[48] In order to simulate the Si-rich phase observed experimentally by Lin et al., we started with the Si-terminated surface. Top of the surface comprises two layers of Si with a height difference of 1.27 Å (Figure 2a). In this model, we first relaxed the top three atomic layers of the [0001] surface of $IrSi_3$. Upon relaxation, these Si layers formed a silicene-like structure with larger Si−Si bond lengths (around 2.4−2.6 Å) and smaller buckling (~0.1 Å) than that of a free-standing silicene.[49] (Figure 2b) We also observed that Si atoms of the silicene layer undergo a significant reconstruction in such a way that after relaxation, the subsurface Ir atoms reside just below the midpoint of Si−Si bonds instead of being right under the Si atoms of the unreconstructed surface (Figure 2c,d). This structural reconstruction helps Ir and Si atoms to saturate their dangling bonds and lower the surface energy.

High-resolution STM images measured on SLDs show that there are six protrusions in the unit cell. The average distance between two nearest neighbor protrusions is about 0.6 nm which is similar to the distance between two Si adatoms on 7 × 7-Si(111) measured under similar tunneling conditions. Following the similarity with the adatoms of Si(111), we elevated some of the Si atoms by an amount of 0.5 Å, so that the model of the surface reflects the symmetry observed in the STM images. However, when we relaxed the system, the elevated Si atoms returned to their original position. On the other hand, under biaxial strain, Si atoms stayed at the elevated positions, suggesting that the observed surface reconstruction is a way to relieve built-up strain. For the calculations presented in this paper, we fixed the elevated Si atoms and relaxed the unelevated Si atoms of SLDs (Figure 3a,b). The

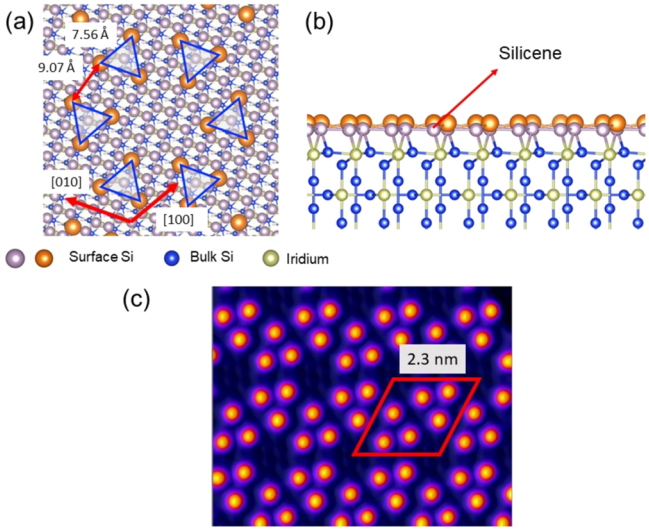

Figure 3. (a) Top and (b) side view of SLDs formed on the reconstructed $IrSi_3$(0001) surface. The red arrows in (a) indicate high-symmetry directions of $IrSi_3$. Orange and violent spheres are used to distinguish silicone atoms of the surface from the bulk Si atoms (blue spheres) of $IrSi_3$. The height difference between orange and violent silicon atoms is about 0.5 Å. The STM image, calculated by integration of states from −1.5 eV to the Fermi level, of SLD is shown in (c). The surface unit cell is also shown by red parallelogram.

lattice parameter of surface reconstruction of $IrSi_3$(0001) is 23.1 Å. The edges of the red rhombus defining the unit cell are parallel to the $\sqrt{7} \times \sqrt{7}$ (with respect to 1 × 1 of Si(111)) unit cell of Ir-ring clusters formed on the Si(111) surface. Therefore, the surface reconstruction of $IrSi_3$(0001) can be described as $2\sqrt{7} \times 2\sqrt{7}$ [with respect to Si(111)]. Upon relaxation, the height difference between the elevated and unelevated Si atoms becomes 0.48 Å, which is close to the buckling of free-standing silicene. Buckling creates a significant contrast in the simulated STM images (Figure 3c).

To reveal electronic properties of the SLDs, we performed STS measurements and calculated DOS with DFT. Both LDOS curves measured on SLDs and the calculated DOS curve exhibit similar features, however the dip measured around the Fermi level in LDOS curve is shifted to 0.3 eV below the Fermi level in the calculated DOS curve (Figure 4a,b). A comparison between peak positions in both graphs also confirms a shift in similar magnitudes in the same direction. Owing to the computational limitations, the DFT calculations were carried out only on the $IrSi_3$ system, and the underlying Si bulk was not considered. IrS_3 islands are surrounded by $\sqrt{7} \times \sqrt{7}$ domains (Figure 1a,b). The $\log(I)-V$ curves measured on $\sqrt{7} \times \sqrt{7}$ domains show that the surface is p-type, whereas the Si bulk is n-type[50] (Figure 4c). This is only possible if the surface has acceptor type of states. Occupied acceptor states carry negative charges and induce upward band bending.[51] If the band bending is strong enough because of high density of surface acceptor states at lower energies in the forbidden band, there can be an inversion layer. For example, on the Si(111)-7 × 7 surface, the surface states (acceptor type) cover almost all the bulk band gap (1.1

DOI: 10.1021/acs.jpcc.9b00550
J. Phys. Chem. C 2019, 123, 7225−7229

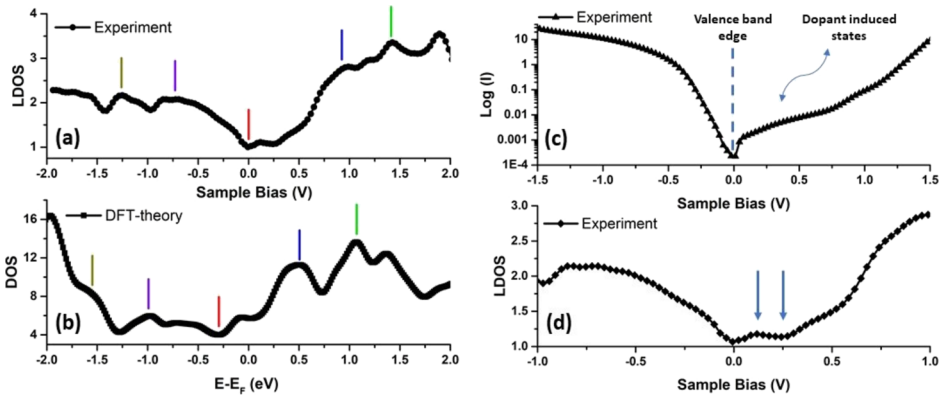

Figure 4. (a) Normalized conductance (LDOS) curve measured on SLDs. (b) DOS of the SLDs calculated with the DFT. Color coded, vertical lines in (a,b) are to show corresponding positions in both graphs. (c) log(I) vs V graph shows p-doped nature of $\sqrt{7} \times \sqrt{7}$ domains. (d) Zoomed-in version of the LDOS shown in (a). Two vertical arrows indicate the position of a peak and dip in the graph.

eV) and create an inversion layer. These surface states pin the Fermi level at about 0.7 eV above the valence band edge leading the formation of an electron depletion layer on n-type Si and a hole depletion layer for p-type Si. The band bending is about 0.4 eV. The p-type nature of the $\sqrt{7} \times \sqrt{7}$ domains suggests occurrence of a situation in a similar nature. However, there is a difference between Si(111)-7 × 7 and $\sqrt{7} \times \sqrt{7}$ domains and that is the later has a band gap of about 0.75 eV, indicating that the $\sqrt{7} \times \sqrt{7}$ domains have the acceptor type of surface states localized closer to the bulk valence band edge. These acceptor states at the interface between $IrSi_3$ crystallites and the surface can acquire more electrons from $IrSi_3$ crystallites to make the Fermi levels the same, leading to the observed downshift of the measured Fermi level of $IrSi_3$ with respect to the one calculated.

The LDOS curve shown in Figure 4d is the same as the one in Figure 4a. We only plot between −1 and 1 V to have a better visual around the Fermi level. Although the LDOS curve presented in Figure 4a and 4d do not exhibit any band gap as it was claimed to be present in the LDOS curves measured on silicene/$MoSi_2$ [ref 29], the LDOS curves of these two systems exhibit similar features. For example, there seems to be a small peak at 0.1 eV, and there is a dip at 0.25 eV. The positions of both the peak and the dip are shifted to lower energies in our system. This can be due to the difference in the electronic properties of the underlying crystallites.

CONCLUSIONS

In this study, we demonstrated a novel method to grow SLDs on Ir-modified Si(111) surface which can pave the way to integrate silicene into silicon-based technologies. After depositing >1 ML of Ir and annealing the surface at 750 °C, $IrSi_3$ crystallites form. Most of the crystallites have featureless morphology, suggesting that they were terminated by the Ir-rich surface of $IrSi_3$. We attribute this to the fact that as crystallites grow, Si atoms must come from the substrate through the crystallites to form the top layers, which limits the supply of Si atoms. As a result of that most of the crystallites terminate with the Ir-rich surface. dI/dV curves measured on these crystallites confirm that they are metallic. On the other hand, some $IrSi_3$ crystallites have SLDs which grow on the top surface similar to a low-buckled silicene. The LDOS curves measured on the SLDs have nonzero density of states around the Fermi level, indicating the metallic nature of the surface. There is a small dip at 0.25 eV. A similar feature was observed on silicene/$MoSi_2$ and silicene/ZrB_2(0001) systems. The dip was suggested to be originating from a gap opening around the Dirac energy; however, these claims, including ours, need to be verified by other methods such as ARPES.

AUTHOR INFORMATION

Corresponding Author

*E-mail: nuri.oncel@und.edu.

ORCID

Deniz Çakır: 0000-0003-3315-5204

Nuri Oncel: 0000-0002-0292-3349

Notes

The authors declare no competing financial interest.

ACKNOWLEDGMENTS

This work was partially supported by the National Science Foundation (DMR-1306101). Computer resources used in this work are provided by Computational Research Center (HPC Linux cluster) at the University of North Dakota. A part of this work was supported by the University of North Dakota Early Career Award (grant number: 20622-4000-02624).

REFERENCES

(1) Castro Neto, A. H.; Guinea, F.; Peres, N. M. R.; Novoselov, K. S.; Geim, A. K. The Electronic Properties of Graphene. *Rev. Mod. Phys.* **2009**, *81*, 109−162.

(2) Weiss, N. O.; Zhou, H.; Liao, L.; Liu, Y.; Jiang, S.; Huang, Y.; Duan, X. Graphene: An Emerging Electronic Material. *Adv. Mater.* **2012**, *24*, 5782−5825.

(3) Le Lay, G.; Salomon, E.; De Padova, P.; Layet, J.-M.; Angot, T. The Rise of Elemental Two-Dimensional Materials Beyond Graphene. *Aust. J. Chem.* **2014**, *67*, 1370.

(4) Bundy, F. P. Phase Diagrams of Silicon and Germanium to 200 kbar, 1000°C. *J. Chem. Phys.* **1964**, *41*, 3809−3814.

(5) Guzmán-Verri, G. G.; Lew Yan Voon, L. C. Electronic Structure of Silicon-Based Nanostructures. *Phys. Rev. B: Condens. Matter Mater. Phys.* **2007**, *76*, 75131.

(6) Takeda, K.; Shiraishi, K. Theoretical Possibility of Stage Corrugation in Si and Ge Analogs of Graphite. *Phys. Rev. B: Condens. Matter Mater. Phys.* **1994**, *50*, 14916−14922.

(7) Yang, X.; Ni, J. Electronic Properties of Single-Walled Silicon Nanotubes Compared to Carbon Nanotubes. *Phys. Rev. B: Condens. Matter Mater. Phys.* **2005**, *72*, 195426.

DOI: 10.1021/acs.jpcc.9b00550
J. Phys. Chem. C 2019, 123, 7225−7229

(8) Durgun, E.; Tongay, S.; Ciraci, S. Silicon and III-V Compound Nanotubes: Structural and Electronic Properties. *Phys. Rev. B: Condens. Matter Mater. Phys.* **2005**, *72*, 075420.
(9) Cahangirov, S.; Topsakal, M.; Aktürk, E.; Şahin, H.; Ciraci, S. Two- and One-Dimensional Honeycomb Structures of Silicon and Germanium. *Phys. Rev. Lett.* **2009**, *102*, 236804.
(10) Liu, C.-C.; Feng, W.; Yao, Y. Quantum Spin Hall Effect in Silicene and Two-Dimensional Germanium. *Phys. Rev. Lett.* **2011**, *107*, 76802.
(11) Aufray, B.; Kara, A.; Vizzini, S.; Oughaddou, H.; Léandri, C.; Ealet, B.; Le Lay, G. Graphene-like Silicon Nanoribbons on Ag(110): A Possible Formation of Silicene. *Appl. Phys. Lett.* **2010**, *96*, 183102.
(12) Cerdá, J. I.; Sławińska, J.; Le Lay, G.; Marele, A. C.; Gómez-Rodríguez, J. M.; Dávila, M. E. Unveiling the Pentagonal Nature of Perfectly Aligned Single-and Double-Strand Si Nano-Ribbons on Ag(110). *Nat. Commun.* **2016**, *7*, 13076.
(13) Chen, L.; Li, H.; Feng, B.; Ding, Z.; Qiu, J.; Cheng, P.; Wu, K.; Meng, S. Spontaneous Symmetry Breaking and Dynamic Phase Transition in Monolayer Silicene. *Phys. Rev. Lett.* **2013**, *110*, 085504.
(14) Qiu, J.; Fu, H.; Xu, Y.; Oreshkin, A. I.; Shao, T.; Li, H.; Meng, S.; Chen, L.; Wu, K. Ordered and Reversible Hydrogenation of Silicene. *Phys. Rev. Lett.* **2015**, *114*, 126101.
(15) Sheng, S.; Wu, J.; Cong, X.; Li, W.; Gou, J.; Zhong, Q.; Cheng, P.; Tan, P.; Chen, L.; Wu, K. Vibrational Properties of a Monolayer Silicene Sheet Studied by Tip-Enhanced Raman Spectroscopy. *Phys. Rev. Lett.* **2017**, *119*, 196803.
(16) Chen, L.; Feng, B.; Wu, K. Observation of a Possible Superconducting Gap in Silicene on Ag(111) Surface. *Appl. Phys. Lett.* **2013**, *102*, 081602.
(17) Meng, S.; Shao, T.-N.; Li, H.; Cheng, P.; Chen, L.; Liu, C.-C.; Yao, Y.; Feng, B.; Wu, K. Observation of Dirac Cone Warping and Chirality Effects in Silicene. *ACS Nano* **2013**, *7*, 9049−9054.
(18) Qiu, J.; Fu, H.; Xu, Y.; Zhou, Q.; Meng, S.; Li, H.; Chen, L.; Wu, K. From Silicene to Half-Silicane by Hydrogenation. *ACS Nano* **2015**, *9*, 11192−11199.
(19) Feng, Y.; Liu, D.; Feng, B.; Liu, X.; Zhao, L.; Xie, Z.; Liu, Y.; Liang, A.; Hu, C.; Hu, Y.; et al. Direct Evidence of Interaction-Induced Dirac Cones in a Monolayer Silicene/Ag(111) System. *Proc. Natl. Acad. Sci. U.S.A.* **2016**, *113*, 14656−14661.
(20) He, Z.; Zhuang, J.; Wang, L.; Feng, H.; Gao, Q.; Xu, X.; Hao, W.; Wang, X.; Zhang, C.; Wu, K.; Dou, S. X.; Chen, L.; Hu, Z.; Du, Y. Realization of Flat Band with Possible Nontrivial Topology in Electronic Kagome Lattice. *Sci. Adv.* **2018**, *4*, No. eaau4511.
(21) Meng, L.; Wang, Y.; Zhang, L.; Du, S.; Wu, R.; Li, L.; Zhang, Y.; Li, G.; Zhou, H.; Hofer, W. A.; Gao, H.-J. Buckled Silicene Formation on Ir(111). *Nano Lett.* **2013**, *13*, 685−690.
(22) Fleurence, A.; Friedlein, R.; Ozaki, T.; Kawai, H.; Wang, Y.; Yamada-Takamura, Y. Experimental Evidence for Epitaxial Silicene on Diboride Thin Films. *Phys. Rev. Lett.* **2012**, *108*, 245501.
(23) Rachid Tchalala, M.; Enriquez, H.; Mayne, A. J.; Kara, A.; Roth, S.; Silly, M. G.; Bendounan, A.; Sirotti, F.; Greber, T.; Aufray, B.; Dujardin, G.; Ait Ali, M.; Oughaddou, H. Formation of one-dimensional self-assembled silicon nanoribbons on Au(110)-(2 × 1). *Appl. Phys. Lett.* **2013**, *102*, 083107.
(24) Feng, B.; Ding, Z.; Meng, S.; Yao, Y.; He, X.; Cheng, P.; Chen, L.; Wu, K. Evidence of Silicene in Honeycomb Structures of Silicon on Ag(111). *Nano Lett.* **2012**, *12*, 3507−3511.
(25) Lin, C.-L.; Arafune, R.; Kawahara, K.; Tsukahara, N.; Minamitani, E.; Kim, Y.; Takagi, N.; Kawai, M. Structure of Silicene Grown on Ag(111). *Appl. Phys. Express* **2012**, *5*, 045802.
(26) Chen, L.; Liu, C.-C.; Feng, B.; He, X.; Cheng, P.; Ding, Z.; Meng, S.; Yao, Y.; Wu, K. Evidence for Dirac Fermions in a Honeycomb Lattice Based on Silicon. *Phys. Rev. Lett.* **2012**, *109*, 56804.
(27) Vogt, P.; De Padova, P.; Quaresima, C.; Avila, J.; Frantzeskakis, E.; Asensio, M. C.; Resta, A.; Ealet, B.; Le Lay, G. Silicene: Compelling Experimental Evidence for Graphenelike Two-Dimensional Silicon. *Phys. Rev. Lett.* **2012**, *108*, 155501.
(28) De Padova, P.; Vogt, P.; Resta, A.; Avila, J.; Razado-colambo, I.; Quaresima, C.; Olivieri, B.; Bruhn, T.; Hirahara, T.; et al. Evidence of Dirac Fermions in Multilayer Silicene. *Appl. Phys. Lett.* **2014**, *102*, 163106.
(29) Volders, C.; Monazami, E.; Ramalingam, G.; Reinke, P. Alternative Route to Silicene Synthesis via Surface Reconstruction on h - MoSi 2 Crystallites. *Nano Lett.* **2017**, *17*, 299−307.
(30) Bampoulis, P.; Zhang, L.; Safaei, A.; van Gastel, R.; Poelsema, B.; Zandvliet, H. J. W. Germanene termination of Ge2Pt crystals on Ge(110). *J. Phys.: Condens. Matter* **2014**, *26*, 442001.
(31) Kresse, G.; Furthmüller, J. Efficiency of Ab-Initio Total Energy Calculations for Metals and Semiconductors Using a Plane-Wave Basis Set. *Comput. Mater. Sci.* **1996**, *6*, 15−50.
(32) Kresse, G. Ab Initio Molecular Dynamics for Liquid Metals. *J. Non-Cryst. Solids* **1995**, *192-193*, 222−229.
(33) Blöchl, P. E. Projector Augmented-Wave Method. *Phys. Rev. B: Condens. Matter Mater. Phys.* **1994**, *50*, 17953−17979.
(34) Perdew, J. P.; Burke, K.; Ernzerhof, M. Generalized Gradient Approximation Made Simple. *Phys. Rev. Lett.* **1996**, *77*, 3865−3868.
(35) Monkhorst, H. J.; Pack, J. D. Special Points for Brillouin-Zone Integrations. *Phys. Rev. B: Solid State* **1976**, *13*, 5188−5192.
(36) Nicholls, D.; Oncel, N. Iridium-Modified Si(111) Surface. *J. Phys.: Condens. Matter* **2013**, *25*, 445004.
(37) Oncel, N.; Çakır, D.; Dil, J. H.; Slomski, B.; Landolt, G. Angle-resolved synchrotron photoemission and density functional theory on the iridium modified Si(1 1 1) surface. *J. Phys.: Condens. Matter* **2014**, *26*, 285501.
(38) Chu, J. J.; Chen, L. J.; Tu, K. N. Localized epitaxial growth of IrSi3on (111) and (001) silicon. *J. Appl. Phys.* **1988**, *63*, 1163−1167.
(39) Demuth, V.; Strunk, H. P.; Wörle, D.; Kumpf, C.; Burkel, E.; Schulz, M. Formation of amorphous layers by solid-state reaction. from thin Ir films on Si(100). *Appl. Phys. A: Mater. Sci. Process.* **1999**, *68*, 451−455.
(40) Knaepen, W.; Demeulemeester, J.; Deduytsche, D.; Jordan-Sweet, J. L.; Vantomme, A.; Van Meirhaeghe, R. L.; Detavernier, C.; Lavoie, C. In Situ X-Ray Diffraction Study of Thin Film Ir/Si Solid State Reactions. *Microelectron. Eng.* **2010**, *87*, 258−262.
(41) Wittmer, M.; Oelhafen, P.; Tu, K. N. Electronic Structure of Iridium Silicides. *Phys. Rev. B: Condens. Matter Mater. Phys.* **1986**, *33*, 5391−5400.
(42) Okamoto, H. Ir-Si (Iridium-Silicon). *J. Phase Equilib. Diffus.* **2007**, *28*, 495.
(43) Zhao, N.; He, Y. Q.; Yang, C. C. A New Approach to Construct Bulk and Size-Dependent Continuous Binary Solution Phase Diagrams of Alloys. *RSC Adv.* **2015**, *5*, 96323−96327.
(44) Wautelet, M.; Dauchot, J. P.; Hecq, M. Phase Diagrams of Small Particles of Binary Systems: A Theoretical Approach. *Nanotechnology* **2000**, *11*, 6−9.
(45) Adhikari, H.; Marshall, A. F.; Chidsey, C. E. D.; McIntyre, P. C. Germanium Nanowire Epitaxy: Shape and Orientation Control. *Nano Lett.* **2006**, *6*, 318−323.
(46) Lin, T. L.; Nieh, C. W.; Hashimoto, S.; Xiao, Q. F. Growth of IrSi3 by molecular beam epitaxy. *Thin Solid Films* **1990**, *184*, 343−348.
(47) From ref 38: type A: $[2\bar{1}\bar{1}0]IrSi_3//[111]Si$, type B: $[0001]IrSi_3//[111]Si$, type C: $[03\bar{3}\bar{1}]IrSi_3//[111]Si$.
(48) Persson, K. *Materials Data on Si_3Ir (SG:194) by Materials Project*. Doi: 10.17188/1204147, United States, 2, 2016.
(49) Cahangirov, S.; Topsakal, M.; Aktürk, E.; Şahin, H.; Ciraci, S. Two- and One-Dimensional Honeycomb Structures of Silicon and Germanium. *Phys. Rev. Lett.* **2009**, *102*, 236804.
(50) Johnson, M. B. Scanning Tunneling Microscopy and Spectroscopy for Studying Cross-Sectioned Si(100). *J. Vac. Sci. Technol., B: Microelectron. Nanometer Struct.–Process., Meas., Phenom.* **1992**, *10*, 508.
(51) Luth, H. *Solid Surfaces, Interfaces and Thin Films*, 4th ed.; Springer, 2001; p 331.

DOI: 10.1021/acs.jpcc.9b00550
J. Phys. Chem. C 2019, 123, 7225−7229